Anal. Chem. **1998,** *70,* 332−339

Monitoring Anhydride and Acid Conversion in Supercritical/Hydrothermal Water by in Situ Fiber-Optic Raman Spectroscopy

Wendy C. Bell,[†] Karl S. Booksh,[‡] and M. L. Myrick*,[†]

Department of Chemistry and Biochemistry, University of South Carolina, Columbia, South Carolina 29208, and Department of Chemistry and Biochemistry, Arizona State University, Tempe, Arizona 85287

The hydrolysis of acetic anhydride to acetic acid in a hydrothermal/supercritical water reactor is monitored via in situ fiber-optic Raman spectroscopy to demonstrate the use of in situ spectroscopy to gain understanding of reaction kinetics and thermodynamics. We discuss the instrumentation used to make measurements in this harsh, corrosive medium, the multivariate mathematical methods used to interpret the spectroscopy, and the mass balance relationships used to convert the result into kinetic and thermodynamic information. From the intensity relationships and temperature information, E_a for the hydrolysis reaction is estimated and compared to literature values. Also, ΔH and ΔS are estimated for a change in solvation environment of acetic acid at high temperatures.

At 300 °C and 3000 psi, the polarity and density of water approach those of acetone at room temperature.[1] As water approaches the critical point (375 °C, 3500 psi), the gradual decrease in its dielectric constant causes an increase in the solubility of organic compounds. In the past decade, incentives such as the low cost and environmental friendliness of supercritical water (SCW) have led to growing interest in the medium as a solvent for chemical reactions. Progress has been especially impressive in the area of the destruction of hazardous organic wastes. Interest has been stimulated by the fact that organic materials can be oxidized cleanly and completely[2] in SCW and the method is simultaneously less costly and less wasteful of resources than traditional methods of digestion.[3] Studies have also aimed at exploring the utility of hydrothermal and SCW as a replacement for many hazardous organic solvents used in organic synthesis.

Despite the potential usefulness of SCW, relatively little is known about the fundamental chemistry of reactions in this medium. In the past, chemical reactivity in supercritical fluids has been mainly investigated by traditional means, analyzing products after the mixture has been returned to ambient conditions. However, some research groups have begun using fluorescence,[4−14] UV−visible,[15,16] infrared absorbance,[16−21] and Raman scattering spectroscopy[21−29] to characterize reactions in situ. Using optical spectroscopy, insight can be gained into reaction paths, important intermediates, and rates of reaction. We report here the use of in situ fiber-optic Raman spectroscopy to measure the kinetics of a reaction in hydrothermal and supercritical water. Raman spectroscopy is ideally suited for SCW studies because of its chemical selectivity and the intrinsically weak Raman signal of water.

For our experiment, the hydrolysis of acetic anhydride into acetic acid was studied to demonstrate that spectral information from a small number of experiments can be used to gain important

[†] University of South Carolina.
[‡] Arizona State University.

(1) Kuhlmann, B.; Arnett, E. M.; Siskin, M. *J. Org. Chem.* **1994**, *59*, 3098−101.
(2) Thomason. T.; Modell, M. *Hazard. Waste* **1984**, *1*, 453.
(3) Modell, M.; Larson, J.; Sobczynski, S. F. *Tappi J.* **1992**, *1*, 195−201.
(4) Zhang, J.; Bright, F. V. *J. Phys. Chem.* **1992**, *96*, 5633−41.
(5) Brennecke, J. F.; Tomasko, D. L.; Peshkin, J.; Eckert, C. A. *Ind. Eng. Chem. Res.* **1990**, *29*, 1682−9.
(6) Brennecke, J. F.; Tomasko, D. L.; Eckert, C. A. *J. Phys. Chem.* **1990**, *94*, 7692−700.
(7) Sun, Y.-P.; Bennett, G.; Johnston, K. P.; Fox, M. A. *Anal. Chem.* **1992**, *64*, 1763−8.
(8) Sun, Y.-P.; Fox, M. A. *J. Phys. Chem.* **1993**, *97*, 282−3.
(9) Tomasko, D. L.; Knutson, B. L.; Pouillot, F.; Liotta, C. L.; Eckert, C. A. *J. Phys. Chem.* **1993**, *97*, 11823−34.
(10) Zhang, J.; Lee, L. L.; Brennecke, J. F. *J. Phys. Chem.* **1995**, *99*, 9268−77.
(11) Rice, J. K.; Niemeyer, E. D.; Bright, F. V. *J. Phys. Chem.* **1996**, *100*, 8499−507.
(12) Heitz, M. P.; Bright, F. V. *J. Phys. Chem.* **1996**, *100*, 6889−97.
(13) Sun, Y.-P.; Bowen, T. L.; Bunker, C. E. *J. Phys. Chem.* **1994**, *98*, 12486−94.
(14) Sun, Y.-P.; Bennett, G.; Johnston, K. P.; Fox, M. A. *J. Phys. Chem.* **1992**, *96*, 10001−7.
(15) Xiang, T.; Johnston, K. P. *J. Phys. Chem.* **1994**, *98*, 7915−22.
(16) Franck, E. U. *Phys. Chem. Earth* **1981**, *13&14*, 65−81.
(17) Kazarian, S. G.; Vincent, M. F.; Eckert, C. A. *Rev. Sci. Instrum.* **1996**, *67*, 1586−9.
(18) Maiella, P. G.; Brill, T. B. *Appl. Spectrosc.* **1996**, *50*, 829−35.
(19) Blitz, J. P.; Yonker, C. R.; Smith, R. D. *J. Phys. Chem.* **1989**, *93*, 6661−5.
(20) Franck, E. U.; Roth, K. *Discuss. Faraday Soc.* **1967**, *43*, 108−14.
(21) Franck, E. U. *Pure Appl. Chem.* **1970**, *24*, 13−30.
(22) Myrick, M. L.; Kolis, J.; Parsons, E.; Chike, K.; Lovelace, M.; Scrivens, W.; Holiday, R.; Williams, M. *J. Raman Spectrosc.* **1994**, *25*, 59−65.
(23) Murata, K.; Irish, D. E.; Toogood, G. E. *Can. J. Chem.* **1989**, *67*, 517−25.
(24) Masten, D. A.; Foy, B. R.; Harradine, D. M.; Dyer, R. B. *J. Phys. Chem.* **1993**, *97*, 8557−9.
(25) Marshall, W. L.; Begun, G. M. *J. Chem. Soc., Faraday Trans. 2* **1989**, *85*, 1963−78.
(26) Irish, D. E.; Jarv, T.; Ratcliffe, C. I. *Appl. Spectros*c. **1982**, *36*, 137−40.
(27) Spohn, P. D.; Brill, T. B. *Appl. Spectros*c. **1987**, *41*, 1152−6.
(28) Spohn, P. D.; Brill, T. B. *J. Phys. Chem.* **1989**, *93*, 6224−31.
(29) Steeper, R. R.; Rice, S. F.; Kennedy, I. M.; Aiken, J. D. *J. Phys. Chem.* **1996**, *100*, 184−9.

S0003-2700(97)00714-2 CCC: $15.00
Published on Web 01/15/1998

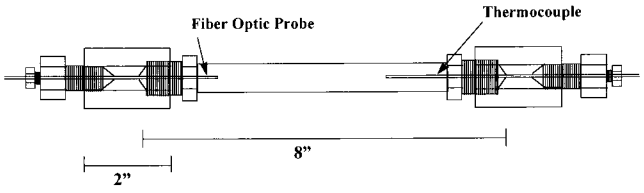

Figure 1. Schematic diagram of reactor.

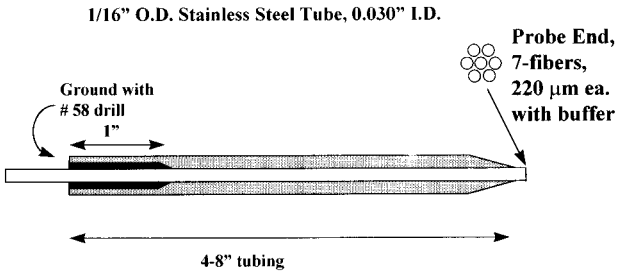

Figure 2. Fiber-optic probe prototype as constructed in this laboratory.

kinetic and thermodynamic information about the nature of a simple reaction in a hydrothermal/supercritical water environment. We also discuss the instrumentation used to make measurements in this harsh, corrosive medium, the multivariate mathematical methods used to interpret the spectroscopy, and the mass balance relationships used to convert the result into kinetic and thermodynamic information. The speed and cost effectiveness of this methodology may prove in situ spectroscopy an efficient tool for the analysis of reactions in challenging pressure/temperature environments.

EXPERIMENTAL SECTION

The design of the probe and 316 stainless steel high-pressure reactor vessel with standard cone and thread fittings is shown in Figure 1. All parts not pertaining directly to the probe are commercially available and were purchased from High Pressure Equipment (Erie, PA). The reactor vessel consists of an 8-in. coned and threaded tube, both ends of which are screwed into reducer coupling. Into one end of the reducer coupling is inserted a $^1/_{16}$-in. 316 stainless steel thermocouple, and the spectroscopic probe is inserted directly opposite. The 8-in. tube and reducer fittings are all pressure rated to 15 000 psi. The 8-in. body of the reactor consisted of a $^9/_{16}$-in.-o.d. pipe, with an i.d. of $^5/_{16}$ in. Samples were loaded by dismantling the reactor, adding the reagents directly to the pipe, and then reassembling. The internal reactor volume was determined to be 10.4 mL. Once the sample was sealed in the reaction vessel, the reactor was placed in a tubular oven at a 40° angle so that the 4 mL of sample covered the probe.

The casing of the high-pressure/high-temperature fiber-optic probe consists of a 4−5-in. piece of $^1/_{16}$-in. 316 stainless steel tubing with flat polished ends. The tubing inner diameter was chosen to match the diameter of the fiber bundle used. To form a high-pressure seal, we aimed for the smallest sealing area possible; hence the fibers were held in place by the physical space restrictions in the steel casing with no additional sealant. The end of the casing that would be outside the reactor was widened by drilling with a No. 58 (0.0420 in.) drill bit ~0.5 in. into the tubing. The fibers were inserted into the length of the tube through the drilled end and JB Weld epoxy filler was used as the sealant only in this part of the casing. The optical fibers used for the studies were 0.22 NA, 200-μm core high-OH step index silica−silica fibers manufactured by Polymicro (Phoenix, AZ) with a total diameter of 250 mm including cladding and buffer layers. Fiber lengths were approximately 2−3 m. For this prototype, a seven fiber, six-around-one, design was used as seen in Figure 2. Two methods for mounting the fibers into the steel jacket were used. In the first (probe design 1), for the final inch of insertion into the casing, epoxy was generously placed on the fibers and then the fibers were drawn into the tubing to their final position. For the second (probe design 2), the fibers were inserted through the length of the casing with 2 in. of fiber extending out of the proximal end. A Bunsen burner flame was used to burn the polyimide jacket from this portion of the fibers. The fibers were then partially drawn back into the casing, epoxy was generously placed on the fibers at the drilled end of the tubing, and the fibers were drawn into the tubing to their final position. Probe design 2 has been successful in eliminating significant background fluorescence in the spectra caused by leaching of the polyimide buffer into the reactor by the supercritical fluid. In both designs, a partial vacuum on the opposite end of the casing further assisted the epoxy into the probe. This pulling of sealant into the widened portion of the probe constituted the high-pressure seal. Because this seal is made in the "cool" zone of the probe, we have found that reactor temperatures above 400 °C and pressures above 4000 psi are easily maintained without probe blow out. The fibers were roughly polished on the probe end, and the probe casing was then electrochemically etched in a 17% H_2SO_4 solution to taper the end and expose 1 mm of fresh fiber. The exposed fiber ends were coated with 5-min epoxy and allowed to set. The fibers were then carefully fine polished and a Bunsen burner was used to burn off the remaining 5-min epoxy. The distal ends of the fibers were inserted into protective jackets and each was terminated with an ST connector (F1-0064, Fiber Instrument Sales, Oriskany, NY). These connectors were linked to other fibers that were kept permanently in alignment with the optics of the system.

The excitation source used was a Spectra Diode Labs (San Jose, CA) 500-mW external cavity diode laser received for β testing. Unfortunately, these lasers are no longer available with a 500-mW power rating. More recently, we have been successfully using a commercially available 300-mW unit by the same manufacturer. However, all the results reported here were acquired with the test unit. A 785-nm band-pass filter (10-nm band-pass) was used to remove broad-band emission from the laser line, and the output beam was focused onto a fiber optic using a Melles Griot (Irvine, CA) diode laser collimating and focusing lens. Near-infrared power was measured with a thermoelectric power meter (Coherent, Model 200) and ranged between 240 and 250 mW at the output end of the fibers.

Prior to sealing the reactor, 2 mL of distilled water and 2 mL of acetic anhydride (5.17 M anhydride) were injected into the reactor. The reactor was placed into the oven, and 30-s exposures were taken consecutively with the internal reactor temperature recorded at each measurement. The Raman scattering was collected via the six surrounding fibers of the in situ fiber-optic

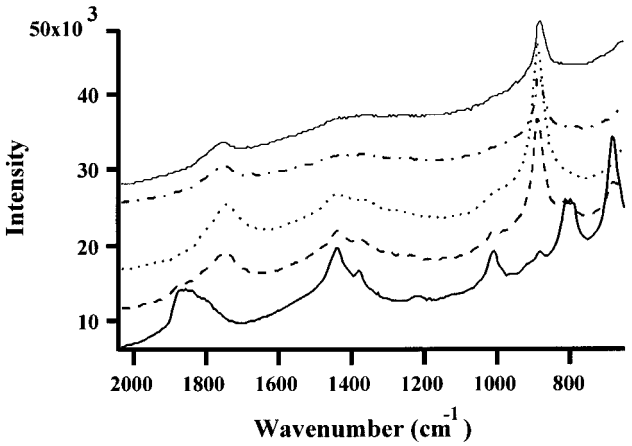

Figure 3. Representative spectra from hydrolysis of acetic anhydride with increasing temperature: (—) 375.3, (—·—) 325.8, (···) 191.3, (– –) 158.9, and (heavy line) 87.3 °C.

probe and directed to a 785-nm holographic notch filter which rejects the laser line. The scattering was then focused into a *f*/2 spectrograph (Laser Raman Systems, Houston, TX) and directed onto a TE cooled CCD detector (Princeton Instruments, Princeton, NJ, Model 1100-PF) equipped with water-cooled jacket. The system was controlled with WinSpec Software on a Gateway 2000 Pentium computer system.

RESULTS AND DISCUSSION

The progress of the hydrolysis of acetic anhydride was observed in situ via fiber-optic Raman spectroscopy during these studies. This reaction is approximately described by

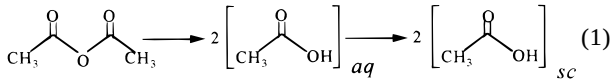

(1)

In this equation, the subscript sc indicates hydrothermal and supercritical solution, while aq has its usual meaning. Figure 3 shows representative spectra from this reaction at several different temperatures.

Evolving factor analysis (EFA) and iterative target transformation factor analysis (ITTFA) were applied to the collected spectra to extract time-dependent concentration profiles of each species encountered during the reaction and the Raman spectrum associated with each species. EFA was originally introduced by Gampp et al. as a method for resolving highly overlapped spectra collected during evolving processes.[30] EFA has been applied to the resolution of liquid chromatographic peaks[31] and ion mobility chromatography mass spectrometry,[32] speciation of metal complexes during titrations and analysis by infrared absorbance,[33] electron spin resonance,[30] UV–visible absorbance,[34] and fluorescence[35,36] spectroscopies. ITTFA is a self-modeling curve resolution technique that is similar to EFA in its ability to resolve highly overlapped, complicated kinetic systems.

Both factor analysis methods decompose a data set **D**, in this case a series of spectra collected during the course of a chemical reaction, into a set of *N* dyads referred to as factors. Here

$$\mathbf{D} = \mathbf{x}_1\mathbf{y}_1^{\mathrm{T}} + \ldots + \mathbf{x}_N\mathbf{y}_N^{\mathrm{T}} + \mathbf{E} = \mathbf{X}\mathbf{Y}^{\mathrm{T}} + \mathbf{E}$$

where *N* columns of **X** are estimates of the true reaction profiles, the columns of **Y** are estimates of the true spectral profiles of the *N* chemical species present during the reaction process, and **E** is a matrix of errors associated with fitting the model to the data. The superscript T denotes the transpose of a matrix or vector. Constraints based on a priori knowledge of the system are placed on the final estimates of **X** and **Y**. Typical constraints are non-negativity of spectral (**Y**) and reaction (**X**) profile estimates and unimodality of reaction profiles (**X**). With EFA, The factors **X** and **Y** are found iteratively by first deriving an initial guess of **X** following principal component analysis (PCA) of **D** then alternately estimating **Y** and **X** while applying the appropriate constraint to the most recent estimate at each step. In this application, only the non-negativities of **X** and **Y** were assumed. The iterative procedure was terminated when the normalized correlation coefficient between successive iterations of **X** and **Y** were both greater than 0.999 999 999.

The initial estimate of composition profiles with ITTFA is found by performing a needle search of the data. In the needle search, test vectors approximating very narrow peaks are fit to the data using a target testing method. After fitting, values for error of the fit for each test vector are calculated and plotted. A local minimum in the error of fit plot corresponds to the test vector locating a maximum in the composition profile for one species. Once the proper number and location of peaks are determined, predicted vectors are computed by a least-squares target testing method.[37] The algorithm for ITTFA was provided by Paul Gemperline at East Carolina University. In this application, the non-negativity of **X** and **Y** and the unimodality of **X** were assumed. The iterative process was terminated when the normalized correlation coefficient of 0.999 999 was reached.

Therefore, the EFA and ITTFA methods applied here differ by (a) the method by which the original estimate of the spectral/concentration profiles are derived and (b) the unimodality constraints applied during each analysis. Both of these methods have advantages over other neural network/pattern recognition methods because they are inherently linear methods applied to a linear data set. Neural network pattern recognition and similar methods are inherently nonlinear and therefore not as suited for this type of data. Further details of factor analysis can be found in the monograph by Malinowski.[38]

Curve Resolution Results. Factor analysis was attempted with two-, three-, and four-factor models. Two-factor models did

(30) Gampp, H.; Maeder, M.; Meyer, C. J.; Zuberbuhler, A. D. *Talanta* **1985**, *32*, 1133.
(31) Maeder, M. *Anal. Chem.* **1897**, *59*, 525–7.
(32) Gemperline, P.; Hamilton, J. C. *J. Chemom.* **1988**, *3*, 455.
(33) Machado, A. A. S. C.; da Silva, J. C. G. E. *Chemom. Intell. Lab. Syst.* **1992**, *17*, 249.
(34) Tauler, R.; Casassas, E. *J. Chemom.* **1988**, *3*, 151.
(35) Silva, C. S. P. C. O.; da Silva, J. C. G. E.; Machado, A. A. S. C. *Appl. Spectrosc.* **1994**, *48*, 363.
(36) da Silva, J. C. G. E.; Machado, A. A. S. C. *Chemom. Intell. Lab. Sys.* **1995**, *27*, 115.
(37) Gemperline, P. J. *Chemometrics Short Course*; East Carolina University, 1996.
(38) Malinowski, E. *Factor Analysis in Chemistry*, 2nd ed.; John Wiley and Sons: New York, 1991.

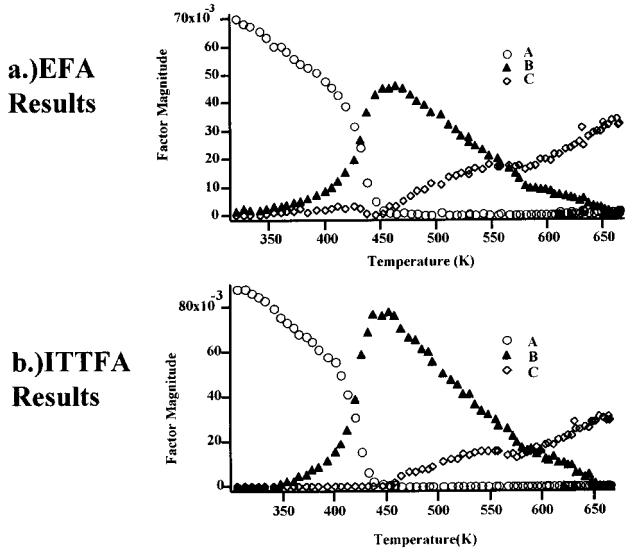

Figure 4. Unadjusted time concentration profiles from three-factor (a) evolving factor analysis and (b) iterative target transformation factor analysis: (○) component A, (▲) component B, and (◇) component C.

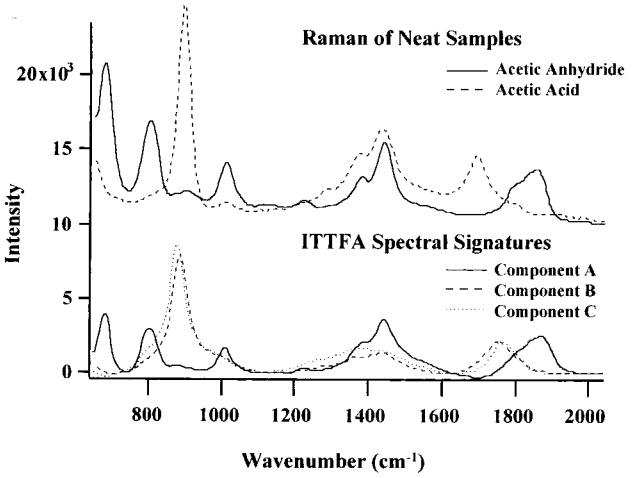

Figure 5. Comparison of spectral signatures from FT Raman and spectra obtained during supercritical/hydrothermal reaction: (—) acetic anhydride, (···) acetic $acid_{aq}$, and (– –) acetic $acid_{sc}$.

Table 1. Peak Assignments of Acetic Anhydride and Acetic Acid Raman Spectra

cm^{-1}	assignment
	Anhydride[39]
677	$A\gamma$ C═O + $A\delta$ C═O
798	$A\nu$ C—C
1009	$A\rho$ CH_3
1441	$A\gamma_{AS}CH_3$
1878	$A\nu$ C═O
	Acid[40]
894	$A\nu$ C—C
1432	$A\nu$ CH_3
1690	$A\nu$ C═O

not sufficiently describe the variance in the spectral data as determined by a visualization of the residuals. With the four-factor model, two of the factors were nearly identical. This is indicative of incorporating one too many factors in the model. Therefore the three factor was deemed most appropriate. This is supported by PCA applied to the data which shows that the eigenvalue associated with the fourth PC was not significant compared to the previous three.

The unadjusted time-dependent concentration profiles derived from the three-factor EFA model and ITTFA model are shown in Figure 4. The results are virtually identical for the two methods, the main difference being a nonzero baseline for the components in EFA. This difference between the two methods is due to the unimodality constraint applied with our ITTFA analysis. We conclude that the choice of starting profiles was immaterial in this case, but the unimodality constraint provided results more consistent with our chemical intuition. The ITTFA profiles were used for all subsequent calculations. In Figure 4b, component A, which is present initially in the reactor, reacts over time to give component B. Component B goes through a maximum concentration and then produces component C. On the basis of a comparison of the spectral signatures derived from the ITTFA model and Raman of neat acetic anhydride and acetic acid, the components A, B, and C are assigned as acetic anhydride, $HOAc_{aq}$, and $HOAc_{sc}$, respectively (Figure 5). Peak assignments based on literature comparison[39,40] are found in Table 1. The noted shift in the peak at 1690 cm^{-1} in the neat acetic acid spectra as compared to the peak at 1780 cm^{-1} in the ITTFA spectral signatures of components B and C is due to solvation effects of water and acetic acid. Experimental titration of acetic acid with water at room temperature to equal volumes reveals a notable shift in the peak at 1690 cm^{-1} as well as the peak around 890 cm^{-1} as revealed in Figure 6. There is a weakening effect of the C—C structural bond and a strengthening of the C═O bond due to hydrogen bonding with water. It is interesting to note that this shift is also seen between components B and C in the ITTFA spectral signatures revealing increased solvation strength for the component C species—counter to our initial expectations.

The profile in Figure 4 cannot be regarded as equivalent to the concentration of each species due to complications caused by changing instrument response and different Raman cross sections for each species. The relationship between concentration and Raman intensity (I) (taken as the ITTFA magnitude) can be described by

$$I_A = [A]f(T)k_A \quad (2)$$

$$I_B = [B]f(T)k_B \quad (3)$$

$$I_C = [C]f(T)k_C \quad (4)$$

where $f(T)$ is the instrument response factor at any temperature T and k_X represents the sensitivity to each component and is proportional to the Raman cross section for each component.

Because this is a closed system, the sum of the concentrations of the components at any one temperature must equal the sum of the concentration of the components at any other temperature. Using the initial temperature, T = 25 °C, as a reference, the

(39) Mirone, P.; Fortunato, B.; Canziani, P. *J. Mol. Struct.* **1970**, *5*, 283—95.
(40) Bertie, J. E.; Michaelian, K. H. *J. Chem. Phys.* **1982**, *77*, 5267—71.

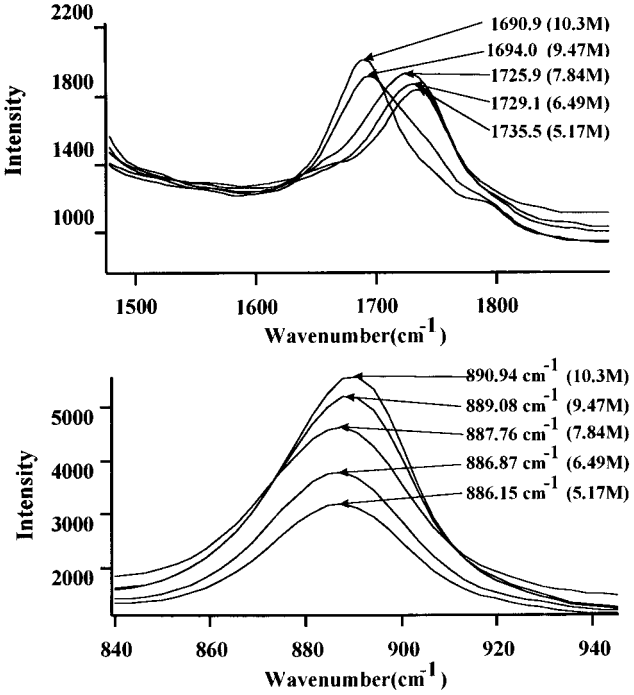

Figure 6. Observed shift in acetic acid Raman peak at 890.94 and 1690.9 cm^{-1} due to change in solvation environment.

concentrations of the three species at any temperature T can be expressed as

$$[A_{25\ ^\circ C}] = [A_T] + [B_T] + [C_T] \quad (5)$$

Substituting the relationships from eqs 2−4 and rearranging, eq 5 expressed in terms of spectral magnitude is

$$I_B = -R_{K1}I_A - I_C/R_{K2} + R_{K1}R_E I_{A_{25\ ^\circ C}} \quad (6)$$

where $R_{K1} = k_A/k_B$, $R_{K2} = k_B/k_C$, and $R_f = f(T_{25°C})/f(T_2)$. R_{K1} is a constant for species in a particular phase and represents the relative sensitivity to species A compared to species B, and similarly, the constant R_{K2} is found as the relative sensitivity to species B compared to species C in a particular phase. R_f is an instrument response factor and accounts for all variability in the measurements due to sampling efficiency. Over most of the reaction, R_f changes gradually. The change in sampling efficiency can be associated with variations in sample density, liquid levels in the reactor and fiber degradation over the course of the reaction. If the change in the response is considered as a function of change in temperature, the result is

$$\frac{\partial I_B}{\partial T} = -\underbrace{\left(R_{K1}\frac{\partial I_A}{\partial T}\right)}_{(1)} - \underbrace{\left(\frac{1}{R_{K2}}\frac{\partial I_C}{\partial T}\right)}_{(2)} + \underbrace{\left(R_{K1}I_{A_{25\ ^\circ C}}\frac{\partial R_f}{\partial T}\right)}_{(3)} \quad (7)$$

At low temperatures early in the reaction, the contribution due to species C is zero in Figure 4. Thus, early in the reaction

$$\partial I_C/\partial T \approx 0$$

eliminating term 2 from eq 7. The third term can also be eliminated from eq 7 because in order to accurately determine R_{K1}, a range of points must be considered where there are appreciable amounts of both species A and B present. This is found over temperatures 384.7−437.8 K. By choosing such a small range of points, we can safely assume that the instrument response factor, R_f is approximately constant. Thus

$$\partial R_f/\partial T \approx 0$$

over this range and term 3 is eliminated from eq 7 resulting in

$$I_B \approx -R_{K1}I_A + \text{const} \quad (8)$$

From this equation, R_{K1} can be found. A plot of I_A vs I_B for the selected experiments yields a straight line with the slope equal to $-R_{K1}$, as seen in Figure 7. R_{K1} is found to have the value +1.131 ± 0.038.

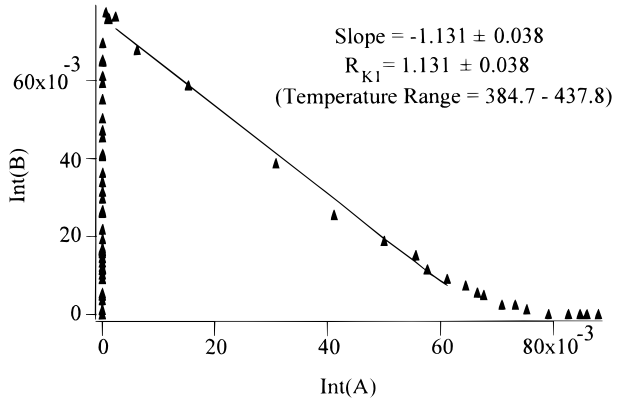

Figure 7. Determination of the relative instrument sensitivity of component B (acetic $acid_{aq}$) to component A (acetic anhydride), R_{K1}.

Similarly, if we consider eq 7 late in the reaction, at high temperatures where most of component A has reacted to yield components B and C,

$$\partial I_A/\partial T \approx 0$$

The first term can therefore be eliminated from the equation and if a similar assumption is made for R_f as was made above, the resulting integrated equation is

$$I_B \approx -(I_C/R_{K2}) + \text{const} \quad (9)$$

A plot of I_B vs I_C yielding a slope of $-(1/R_{K2})$ is shown in Figure 8. Two linear regions of different slope are apparent. This is interpreted as a step change in the relative response to compounds B and C. Because the temperature at which this change occurs is subcritical for water, we believe the change in R_{K2} is due to a change in the partitioning of HOAc between phases under these conditions. For experiments in the temperature range of 458.3−535.4 K, the R_{K2} value is found to be 0.355 ± 0.0142. Once the sensitivity ratio changes, the second region of linearity yields a

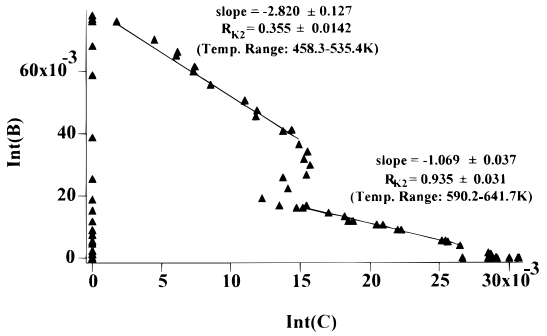

Figure 8. Determination of the relative instrument sensitivity of component C (acetic $acid_{sc}$) to component B (acetic $acid_{aq}$), R_{K2}.

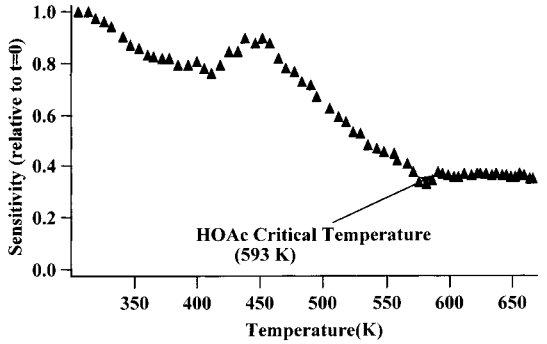

Figure 9. Variation in instrument sensitivity, R_f, with increasing temperature based on observed Raman signal.

value of 0.935 ± 0.031 for R_{K2}. This region includes the temperature range 590.2−641.7 K. For the region of rapid change involving temperatures 590.2−641.7 K, a linear change in relative response from 0.355 to 0.935 was assumed.

Appropriate values for R_{K1} and R_{K2} were then substituted into eq 6 for each temperature range and this was solved for R_f relative to time $t = 0$. A plot of R_f values vs temperature is shown in Figure 9. The calculated instrument response factors (R_f) fall above 440 K until a temperature of 593 K is reached, at which temperature R_f stabilizes. The temperature 593 K coincides with the critical temperature of acetic acid. The expected terminal value of R_f (based on the expansion of a 4-mL volume into the 10.5-mL reactor) is (4/10.5), or 0.381. We obtained an experimental value for the terminal instrument response factor of 0.350 ± 0.002. R_{K1} and R_{K2} are thus found to be state-dependent constants that go through step changes at a phase boundary.

Once the values were calculated for each of the sensitivity parameters of eq 6 (R_{K1}, R_{K2}, R_f), the relative concentrations of each of the components were back calculated from the ITTFA results. (Figure 10).

Thermodynamic Calculations. The result of the preceding exercise is a determination of concentrations of three species over a wide range of temperatures. A number of chemically relevant estimations can be made from data of this type. The reader will recognize that the calculations that follow make implicit assumptions about the state of the system (e.g., that Arrhenius pre-exponential factors and the activity of water remains constant over a 40 deg temperature range). These implicit assumptions are not,

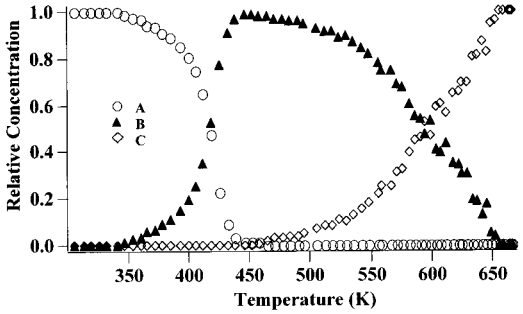

Figure 10. Relative concentrations of species with increasing temperature from Raman: (○) component A, (▲) component B, and (◇) component C.

strictly speaking, correct; additional experiments at different densities, etc., would be needed to more precisely quantify the parameters we estimate. Nevertheless, the data at hand are sufficient for a rapid survey of the thermodynamics of this system, provided the results are taken as approximate.

We begin by estimating the activation barrier for the dissociation of acetic anhydride. This can be obtained from the Arrhenius equation:

$$\ln k = \ln A_o - E_a/RT \tag{10}$$

In this calculation the first-order rate constant k is defined by

$$-k[\mathrm{A}] = \mathrm{d}[\mathrm{A}]/\mathrm{d}t \tag{11a}$$

or

$$k = \frac{-(\mathrm{d}[\mathrm{A}]/[\mathrm{A}])}{\mathrm{d}t} = \frac{\mathrm{d}\ln[\mathrm{A}]}{\mathrm{d}t} \tag{11b}$$

ITTFA provides, ultimately, our estimate of concentration. Consequently, our calculated concentrations are no better than the ITTFA. The reliability of component contributions at low concentrations are not as accurate due to the low signal-to-noise ratios of these components when compared to spectra of more concentrated species. To minimize the effect this has on our thermodynamic calculations, we only consider data with concentrations between 0.9 and 0.1 in our plots. The experiments over which the concentration of A is in this range fall between temperatures of 378.4 and 432.0 K. A plot of ln k vs $1/T$ yields a line as shown in Figure 11a. A linear fit of these data allow the slope over this temperature range to be determined and activation energy to be calculated. The activation energy for the hydrolysis of acetic anhydride over this temperature range was found as 102.080 ± 7.84 kJ/mol. An additional experiment was performed in which the temperature was slowly ramped over this region of interest in order to generate more data points over the region and ensure a more reliable E_a calculation. This curve is presented in Figure 11b and also yields an E_a value of 102.61 ± 4.86 kJ/mol over a similar temperature range. In Figure 12, we plot the calculated activation energy for our temperature range vs literature values made at or around room temperature.[41] Extrapolation from the

(41) Koskikallio, J.; Pouli, D.; Whalley, E. *Can. J. Chem.* **1959**, *37*, 1360−6.

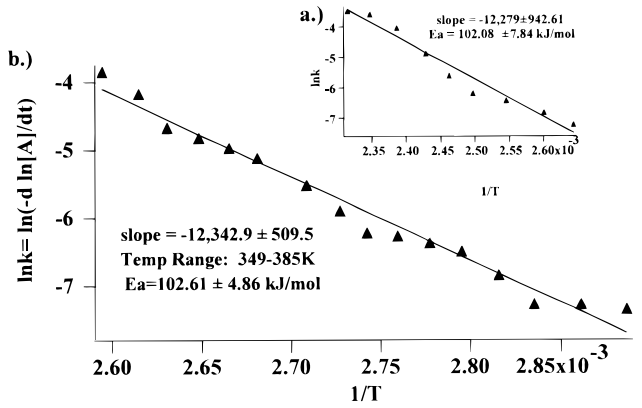

Figure 11. From Arrhenius relationship, ln *k*, as determined from Raman, vs 1/*T* (a) for the temperature range 378.4−432.0 K and (b) for the temperature range 346.4−385.5 K using a slow temperature ramp.

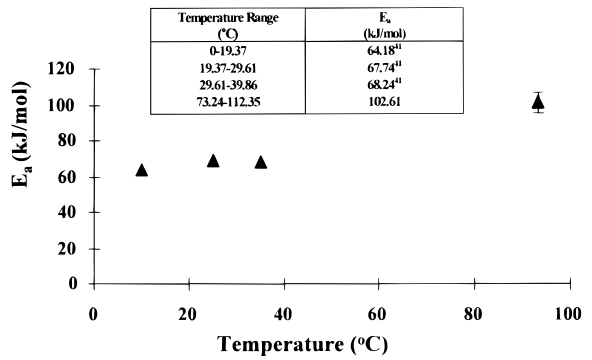

Figure 12. Comparison of our calculated E_a values with literature values around room temperature.[41]

literature values reveal our data points to have a linear relationship with the literature data.

We note in passing that our value of E_a is consistent with the literature value of "acid-catalyzed" hydrolysis, which condition seems appropriate for comparison. However, our literature source reports significantly lower activation barriers for the "noncatalyzed" process. This runs counter to the usual conception of catalysis as a process by which activation barriers are reduced. If ref 41 is correct, then the simple anhydride hydrolysis may have some interesting physical chemistry to disclose yet.

Turning to the process that converts B → C, we found that the major product of the reaction was acetic acid. Since we can clearly identify the ITTFA spectrum of component B as that of acetic acid, component C must be a product that can reversibly return to B. For this reason, we assigned component B as acetic acid in aqueous solution and component C as acetic acid in the hydrothermal/supercritical environment. This begs the question of what, chemically, component C is. Spectroscopic evidence suggests that it represents a differently solvated form of acetic acid, but there are other possibilities as well, including deprotonated acetic acid. From the evidence that component C becomes dominant at high temperature, we conclude that the transformation of B → C (aq → sc) is an endothermic equilibrium process driven to the right at high temperature. If this is indeed an equilibrium process, we can use the apparent equilibrium constant to extract thermodynamic information about the process. To obtain a zeroth order estimate of the enthalpic and entropic cost

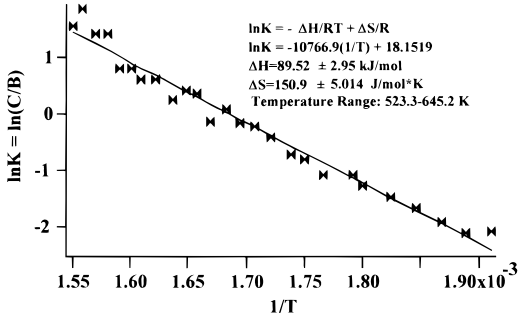

Figure 13. Plot of ln *K* vs 1/*T* for the temperature range 590.2−645.2 K. Information from the fit of this curve is used to approximate ΔH and ΔS over this temperature range.

of this reaction, we can use the simple relationship

$$\ln K = -\frac{\Delta H}{RT} + \frac{\Delta S}{R}$$

where *K* is defined as

$$K \approx [\mathrm{C}]/[\mathrm{B}]$$

and describes the process

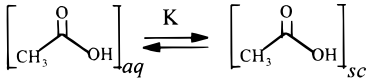

(13)

A plot of ln *K* vs 1/*T* yields the curve as seen in Figure 13. Before the critical point is reached, enthalpy calculations are complicated by change in density of the medium in a two-phase solution. If we focus only on experiments in the region of 590.2−645.2 K (after the critical point of acetic acid has been reached), this complication is removed because the medium occupies the entire volume of the reactor and density is constant. A linear fit of the data in Figure 13 allows the slope to be determined and ΔH is calculated to be 108.4 kJ/mol. Similarly ΔS is calculated from the intercept of the line in Figure 13 and is found to have a value of 182.4 J/(mol K).

CONCLUSIONS

In conclusion, we have investigated an important method for extracting kinetic and thermodynamic information of organic reactions in a challenging medium using a combination of in situ spectroscopy and mathematical interpretation. The usefulness of this method has been demonstrated through the monitoring and characterization of a simple hydrolysis reaction. This four step method can be summarized as (1) making spectroscopic measurements of a single nonisothermal reaction, in our case via in situ fiber optic Raman spectroscopy; (2) mathematically extracting reaction profiles, in our case through evolving factor analysis and iterative target transformation factor analysis; (3) converting the profiles from intensity relationships to relative concentration relationships by applying appropriate boundary conditions; and (4) extracting the thermodynamic information from the calculated concentration and temperature data.

The time investment required to record and interpret the data from the in situ measurements is small once the initial investment required to learn the procedure is made. Based on experience in our laboratory, we believe 3−6 months of effort would be the necessary effort to give most laboratories in the industrial community the capability to measure and interpret data of complexity comparable to those presented here. After this startup cost, experiments and their complete interpretation can often be done in a single day. This estimation is appropriate in laboratories with at least one applied spectroscopist, but little expertise in chemometrics. A different mix of skills and talents could revise the initial cost in either direction.

ACKNOWLEDGMENT

We thank Dr. Tom Bryson for his many useful conversations, Paul Gemperline for his expertise and instruction on chemometrics, and Unilever, Inc. (Edgewater, NJ) for their support for materials used in this project.

Received for review July 7, 1997. Accepted October 22, 1997.[⊗]

AC9707141

[⊗] Abstract published in *Advance ACS Abstracts,* December 15, 1997.